batteries

MDPI

Article

Dehydrogenation of Alkali Metal Aluminum Hydrides $MAlH_4$ (M = Li, Na, K, and Cs): Insight from First-Principles Calculations

Rui Zhou [1], Xiaohua Mo [2], Yong Huang [1], Chunyan Hu [1], Xiaoli Zuo [1], Yu Ma [1], Qi Wei [1] and Weiqing Jiang [1,*]

[1] School of Physical Science & Technology, State Key Laboratory of Featured Metal Materials and Life-Cycle Safety for Composite Structures, Guangxi University, Nanning 530004, China
[2] School of Mathematics and Physics, Key Laboratory for Ionospheric Observation and Simulation, Guangxi University for Nationalities, Nanning 530006, China
* Correspondence: wqjiang@gxu.edu.cn

Abstract: Complex aluminum hydrides with high hydrogen capacity are among the most promising solid-state hydrogen storage materials. The present study determines the thermal stability, hydrogen dissociation energy, and electronic structures of alkali metal aluminum hydrides, $MAlH_4$ (M = Li, Na, K, and Cs), using first-principles density functional theory calculations in an attempt to gain insight into the dehydrogenation mechanism of these hydrides. The results show that the hydrogen dissociation energy (E_d-H_2) of $MAlH_4$ (M = Li, Na, K, and Cs) correlates with the Pauling electronegativity of cation M (χ_P); that is, the E_d-H_2 (average value) decreases, i.e., 1.211 eV ($LiAlH_4$) < 1.281 eV ($NaAlH_4$) < 1.291 eV ($KAlH_4$) < 1.361 eV ($CsAlH_4$), with the increasing χ_P value, i.e., 0.98 (Li) > 0.93 (Na) > 0.82 (K) > 0.79 (Cs). The main reason for this finding is that alkali alanate $MAlH_4$ at higher cation electronegativity is thermally less stable and held by weaker Al-H covalent and H-H ionic interactions. Our work contributes to the design of alkali metal aluminum hydrides with a favorable dehydrogenation, which is useful for on-board hydrogen storage.

Keywords: first-principles calculations; alkali metal aluminum hydrides; cation electronegativity; dehydrogenation performance; electronic structure

check for updates

Citation: Zhou, R.; Mo, X.; Huang, Y.; Hu, C.; Zuo, X.; Ma, Y.; Wei, Q.; Jiang, W. Dehydrogenation of Alkali Metal Aluminum Hydrides $MAlH_4$ (M = Li, Na, K, and Cs): Insight from First-Principles Calculations. *Batteries* **2023**, *9*, 179. https://doi.org/10.3390/batteries9030179

Academic Editors: Chu Liang, Shaohua Lu and Thomas Wetzel

Received: 14 January 2023
Revised: 28 February 2023
Accepted: 15 March 2023
Published: 19 March 2023

Copyright: © 2023 by the authors. Licensee MDPI, Basel, Switzerland. This article is an open access article distributed under the terms and conditions of the Creative Commons Attribution (CC BY) license (https://creativecommons.org/licenses/by/4.0/).

1. Introduction

The rapidly diminishing supply of fossil fuel and increasing environmental awareness have precipitated a growing demand for clean, safe, and renewable energy. Hydrogen is believed to be an ideal clean energy carrier due to its abundance, high energy density (142 MJ/kg), and clean combustion [1]. However, hydrogen is a highly flammable, explosive, and diffusible gas at room temperature and pressure. Thus, it is very important to store hydrogen safely and effectively, yet this task remains a major challenge in hydrogen utilization [2]. Currently, hydrogen storage approaches involve the storage of: (1) compressed hydrogen in high-pressure containers, (2) liquid hydrogen in cryogenic tanks, and (3) hydrogen in solid-state materials via physisorption/chemisorption. Among these approaches, solid-state hydrogen storage provides high hydrogen capacity, moderate operating pressures and temperatures, and favorable safety, and is a promising storage solution [3–5].

Complex metal hydrides, such as alanates, borohydrides, and amides, are considered good solid-state hydrogen storage candidates for on-board applications due to the high gravimetric and volumetric hydrogen densities required in this regard [3,4]. These complex hydrides, unfortunately, are often thermodynamically very stable and dehydrogenate at extremely high temperatures, thereby restricting their practical applications. To overcome these drawbacks, many investigations have been devoted to tuning the thermodynamic properties of complex metal hydrides [6–10].

Nakamori et al. [11] systematically investigated the thermodynamical stabilities of a series of metal borohydrides, $M(BH_4)_n$ (M = Li, Na, K, Cu, Mg, Zn, Sc, Zr, and Hf; n = 1–4),

via first-principles calculations combined with an experimental study. They reported that the stability of $M(BH_4)_n$ is related to the ionic interaction between M and the $[BH_4]$ complex, the charge transfer from the cation M^{n+} to the anion $[BH_4]^-$ ($M^{n+} \rightarrow [BH_4]^-$), and the Pauling electronegativity of the cation M. In particular, a gradual increase in cation Pauling electronegativity χ_P is accompanied by a linear decrease in the dehydrogenation temperature (T_d). Their works on other borohydrides, $M(BH_4)_n$ (M = Ca, Sc, Ti, V, Cr, Mn, Zn, and Al; n = 2–4), also revealed a linear relation between χ_P and T_d [12]. These works by Nakamori and co-workers contribute to the design of metal borohydrides with appropriate stability for favorable dehydrogenation through the combination of $M(BH_4)_n$ with more electronegative metals or metal compounds, which is useful for hydrogen storage applications [6,13–18].

Recently, in the review by Weidenthaler, the decomposition temperature (T_d) of alkali metal aluminum hydrides (alkali alanates) of the $MAlH_4$ variety (M = Li, Na, K, and Cs) is reported to decrease linearly with the Pauling electronegativity, χ_P, of alkali cations [19]. As an example from this review, the decrease in the starting decomposition temperature (the first step of dehydrogenation reaction), specifically, from 443 K ($LiAlH_4$) [20] < 503 K ($NaAlH_4$) [21] < 573 K ($KAlH_4$) [20] < 600 K ($CsAlH_4$) [19], is accompanied by an increase in cation Pauling electronegativity, specifically, from 0.98 (Li) > 0.93 (Na) > 0.82 (K) > 0.79 (Cs). From these results, the electronegativity of alkali metal cations was identified as dominant with respect to the thermal stability and the decomposition temperature of $MAlH_4$ (M = Li, Na, K, and Cs) [19]. However, the dehydrogenation mechanism of $MAlH_4$ associated with cation electronegativity was not provided in the review. Furthermore, to date, there have only been a few reports on this topic. Therefore, in this study, we apply first-principles density functional theory calculations on $MAlH_4$ (M = Li, Na, K, and Cs) since the calculations can reliably be used to study the micro-mechanisms of hydrogen storage materials [11,22,23]. The formation enthalpy, cohesive energy, Hirshfeld charge, hydrogen dissociation energy, density of states, charge density distribution, and Mulliken population of $MAlH_4$ (M = Li, Na, K, and Cs) are investigated in detail. We believe that our work can provide new insights into the dehydrogenation of $MAlH_4$ (M = Li, Na, K, and Cs) and is, therefore, helpful for exploring solid-state alkali aluminum hydrides with favorable H-desorption properties for hydrogen storage applications.

2. Computational Details

The present calculations on the alkali alanates of $MAlH_4$ (M = Li, Na, K, and Cs) were executed using the density functional theory (DFT) method with on-the-fly generation (OTFG) ultrasoft pseudopotential, as implemented in the Cambridge Serial Total Energy Package (CASTEP) code in Materials Studio 2017 [24]. The exchange-correlation function was used with the generalized gradient approximation (GGA)of Perdew–Burke–Ernzerhof (PBE) [25]. The dependence of total energy on the plane–wave cutoff energy and Monkhorst–Pack k-point mesh were tested carefully. Subsequently, a plane–wave cutoff energy of 900 eV and a k-point grid of 3 × 2 × 2 were adopted, thereby ensuring a convergence accuracy with a total energy difference below 3 meV/atom. Atomic valence electrons, namely, $1s^2 2s^1$ (Li), $2s^2 2p^6 3s^1$ (Na), $3s^2 3p^6 4s^1$ (K), $5s^2 5p^6 6s^1$ (Cs), $3s^2 3p^1$ (Al), and $1s^1$ (H), were used for corn electrons. Geometry optimization using the Broyden–Fletcher–Goldfarb–Shanno (BFGS) method [26] allowed the lattice and all atoms to relax, with the convergence tolerance of 1.0×10^{-5} eV/atom, 0.03 eV/Å, 0.05 GPa, and 0.001 Å for energy, maximum force, maximum stress, and maximum displacement, respectively. The single-point energies and electronic structures of all the considered systems were calculated following geometric optimization.

The alkali metal aluminum hydrides of $MAlH_4$ (M = Li, Na, K, and Cs) considered in our studies have space groups of P21/C (monoclinic structure, $LiAlH_4$) [27], I41/A (tetragonal structure, $NaAlH_4$) [28], and Pnma (orthorhombic structure, $KAlH_4$ and $CsAlH_4$) [29,30], as shown in Table 1. The geometric optimization of these aluminum hydrides gave the relaxed lattice parameters and volume (Table 1), whose level of agreement with the experi-

mental data [27–30] is fairly high. Using relaxed $MAlH_4$, a 2 × 1 × 1 supercell consisting of 8 $MAlH_4$ units ($M_8Al_8H_{32}$) was established for calculations, as illustrated in Figure 1. In this figure, two [AlH_4] units in $MAlH_4$ bulk are considered for hydrogen desorption, with their H atoms labeled as H_A, H_B, H_C, H_D, H_E, H_F, and H_G, and Al-H and H-H distances within 1.625–1.643 Å(Al-H) and 2.639–2.754 Å(H-H) in each [AlH_4] unit. From these Al-H and H-H distances, the H bonding (Al-H and H-H bonding) in the [AlH_4] group can be predicted [31]. The previous experimental and theoretical studies on aluminum hydrides also provide support for the formation of Al-H and H-H bonds in the [AlH_4] unit [31–33].

Table 1. The space group (SP), relaxed lattice parameters (R) and cell volume (V), formation enthalpy (ΔH), cohesive energy (E_{coh}), charge transfer from cation M to anion [AlH_4] (C), and alkali cation electronegativity (χ_P) of $MAlH_4$ (M = Li, Na, K, and Cs).

Compounds	SP	R (Å)			V (Å^3)	ΔH (kJ/mol)	E_{coh} (kJ/mol)	C (e)	χ_P
		a	b	c					
$LiAlH_4$	P21/C	4.908	8.031	7.953	289.762	−117.156	−1684.32	0.21	0.98
$NaAlH_4$	I41/A	4.986	4.986	11.178	277.905	−120.468	−1684.704	0.28	0.93
$KAlH_4$	Pnma	8.896	5.810	7.399	382.448	−157.2	−1719.552	0.35	0.82
$CsAlH_4$	Pnma	10.018	6.163	8.077	498.704	−171.9	−1740.768	0.42	0.79

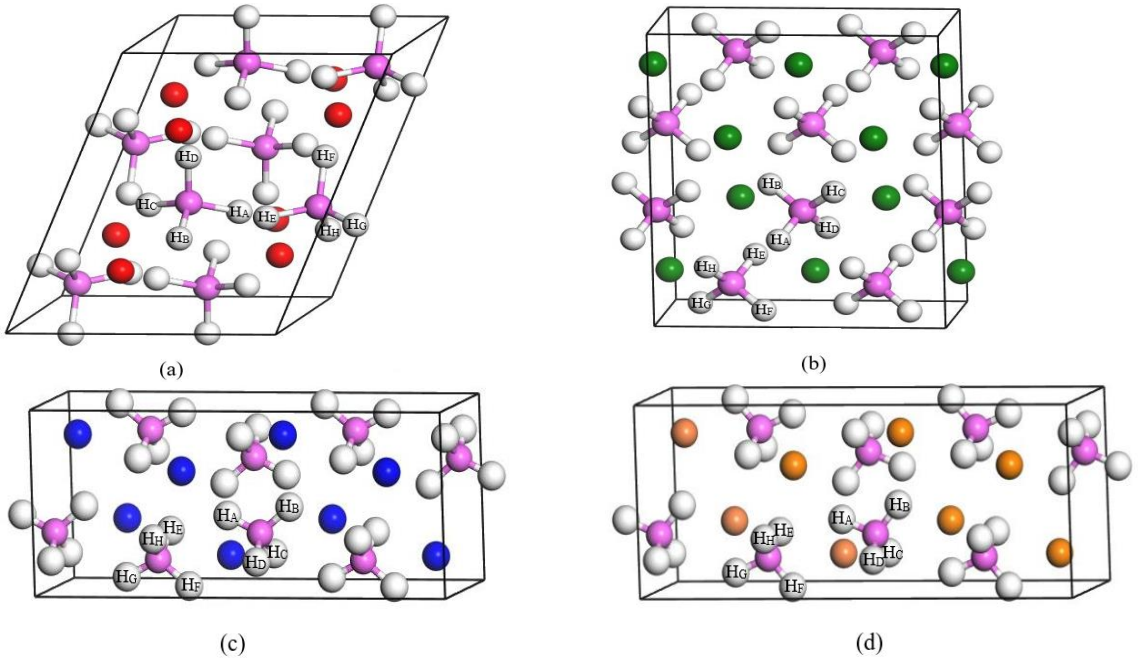

Figure 1. The crystal models of $MAlH_4$ (M = Li, Na, K, and Cs) with 2 × 1 × 1 supercell: (**a**) $LiAlH_4$, (**b**) $NaAlH_4$, (**c**) $KAlH_4$, and (**d**) $CsAlH_4$. Li, Na, K, Cs, Al, and H atoms are denoted by red, green, blue, orange, pink, and white spheres, respectively. The H atoms labeled as H_A, H_B, H_C, H_D, H_E, H_F, H_G, and H_H in two [AlH_4] units are considered for hydrogen desorption.

The formation enthalpy (ΔH) and cohesive energy (E_{coh}) of $MAlH_4$ aluminum hydrides ($LiAlH_4$, $NaAlH_4$, $KAlH_4$, and $CsAlH_4$) are calculated using the following formulae (Equations (1) and (2)), wherein the zero-point energy (ZPE) correction has been considered [34]:

$$\Delta H = E(MAlH_4) - E(M) - E(Al) - 2E(H_2) \quad (1)$$

$$E_{coh} = E(MAlH_4) - \varepsilon(M) - \varepsilon(Al) - 4\varepsilon(H) \quad (2)$$

where $E(MAlH_4)$ denotes the total energy of $MAlH_4$ (M = Li, Na, K, and Cs); E(M/Al) represents the energy of M/Al atom in each crystal structure of bcc-Li/Na/K/Cs and fcc-Al;

ε(M/Al/H) denotes the isolated M/Al/H atom's energy. E(H_2), the energy of hydrogen molecular, is estimated to be −31.407 eV by placing two H atoms 0.741 Åapart [35] in a 10 × 10 × 10 Å (1000 $Å^3$) cubic box. The result is in good agreement with those of −31.292 eV [36] and −31.592 eV [37] from the literature.

The hydrogen dissociation energy is defined as the energy cost of removing hydrogen molecules (hydrogen pair) from the mother bulk, since the initial decomposition of $MAlH_4$ (M = Li, Na, K, and Cs) takes place via the reaction of $3MAlH_4 \rightarrow M_3AlH_6 + 2Al + 3H_2$ with the release of hydrogen gas [19,38,39]. In this case, the hydrogen pairs used for H-dissociation include (H_A and H_B), (H_A and H_C), and (H_A and H_D) from one [AlH_4] unit, and (H_A and H_E), (H_A and H_F), (H_A and H_G), and (H_A and H_H) from two [AlH_4] units (Figure 1). In addition, the two hydrogen atoms, H_A and H_X (H_B, H_C, H_D, H_E, H_F, H_G or H_H), in these hydrogen pairs can be removed in two possible ways: (1) H_A and H_X are taken away one by one (asynchronous hydrogen desorption, expressed as $H_A \rightarrow H_X$). That is, the atom H_A is first removed from the $M_8Al_8H_{32}$ bulk forming $M_8Al_8H_{31}$ with a H_A vacancy, and then atom H_X is removed from relaxed $M_8Al_8H_{31}$ bulk forming $M_8Al_8H_{30}$ with H_A and H_X vacancies. In this case, the hydrogen dissociation energy is calculated by Equation (3) (the first step for H_A removal, E_d-H_A), Equation (4) (the second step for H_X removal, E_d-H_X), and Equation (5) (the total energy for $H_A \rightarrow H_X$ removal, E_d-H_2); (2) H_A and H_X are taken away simultaneously (synchronous hydrogen desorption, denoted as H_A–H_X), with the hydrogen dissociation energy (E_d-H_2) determined by the following Equation (6) [40]

$$E_d - H_A = [E(M_8Al_8H_{31}) + \frac{1}{2}E(H_2)] - E(M_8Al_8H_{32}) \quad (3)$$

$$E_d - H_X = [E(M_8Al_8H_{30}) + \frac{1}{2}E(H_2)] - E(M_8Al_8H_{31}) \quad (4)$$

$$E_d - H_2 = (E_d - H_A) + (E_d - H_X) \quad (5)$$

$$E_d - H_2 = [E(M_8Al_8H_{30}) + E(H_2)] - E(M_8Al_8H_{32}) \quad (6)$$

in which E(H_2) is the same as the previous definition; E($M_8Al_8H_{32}$), E($M_8Al_8H_{31}$), and E($M_8Al_8H_{30}$) are the total energy of corresponding systems.

3. Results and Discussion

3.1. Thermal Stability

The formation enthalpy, ΔH, refers to the formation heat in a hydriding reaction and is helpful for evaluating the thermal stability of metal hydrides [41,42]. A negative formation enthalpy (ΔH < 0) suggests an exothermic reaction. Furthermore, a compound is more thermally stable if it has a more negative formation enthalpy [41–43]. Table 1 lists the formation enthalpy of $MAlH_4$ (M = Li, Na, K, and Cs) with ZPE correction. It has been found that the formation enthalpies, ΔH, of $MAlH_4$ (M = Li, Na, K, and Cs) are always negative, and the values −117.156 kJ/mol ($LiAlH_4$), −120.468 kJ/mol ($NaAlH_4$), −157.2 kJ/mol ($KAlH_4$) and −171.9 kJ/mol ($CsAlH_4$) are in reasonable agreement with the available literature findings, that is, −113.42 kJ/mol ($LiAlH_4$) [44], −155.5 kJ/mol ($NaAlH_4$) [45], and −183.7 kJ/mol ($KAlH_4$) [45]. In particular, these ΔH values become more negative when the Pauling electronegativity of cation M (χ_P, Table 1) decreases, with a linear relation $\Delta H = 296.033\chi_P - 402.19$ obtained via least square fitting in Figure 2. A similar linear correlation, $\Delta H = 248.7\chi_P - 390.8$, is also presented in borohydrides [11]. It is clear from the results above that $MAlH_4$ (M = Li, Na, K, and Cs) aluminum hydrides may have reduced negative formation enthalpy as their alkali cation M has greater electronegativity, such as ΔH = −117.156 kJ/mol and χ_P = 0.98 for $LiAlH_4$ vs. ΔH = −171.9 kJ/mol and χ_P = 0.79 for $CsAlH_4$. The cohesive energy E_{och} (Table 1), interestingly, has the same characteristics as the formation enthalpy ΔH, for which a linear relationship between E_{och} and χ_P, $E_{coh} = 296.489\chi_P - 1968.247$, is also achieved. These ΔH and E_{och} results suggest

that the thermal stability corresponds to a descending order, wherein $LiAlH_4$ < $NaAlH_4$ < $KAlH_4$ < $CsAlH_4$ [41–43,46], followed by the decomposition temperature [11,19].

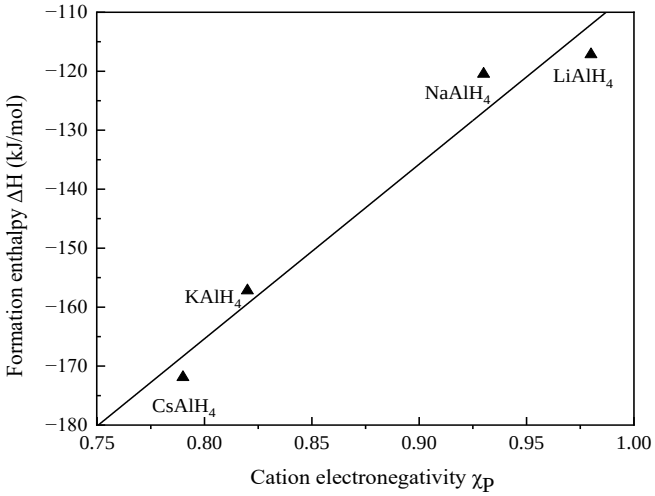

Figure 2. The formation enthalpy (ΔH) as a function of cation electronegativity (χ_P) for $MAlH_4$ (M = Li, Na, K, and Cs) alanates. The straight line, $\Delta H = 296.033\chi_P - 402.19$, indicates least square fitting.

The charge transfer of a metal cation is related to its electronegativity, and it can help assess the thermal stability of metal hydrides. As mentioned in [11,47,48], the $M^{n+} \rightarrow [BH_4]^-$ charge transfer is an important characteristic of the stability of $M(BH_4)_n$ borohydrides. The suppression of the charge transfer by the substitution of a metal cation with a more electronegative element is expected to tailor the stability, thereby effectively lowering the dehydrogenation temperature of borohydrides. In this regard, it is interesting to find that the $M^+ \rightarrow [AlH_4]^-$ charge (Hirshfeld charge) transfer increases from 0.21 e ($LiAlH_4$) to 0.28 e ($NaAlH_4$), 0.35 e ($KAlH_4$), and 0.42 e ($CsAlH_4$), with the cation electronegativity (χ_P) decreasing from 0.98 (Li) to 0.93 (Na), 0.82 (K), and 0.79 (Cs), as shown in Table 1. The results indicate that the increase in cation electronegativity helps to suppress the charge transfer of the alkali cation; as a consequence, the thermal stability of $MAlH_4$ (M = Li, Na, K, and Cs) is reduced [11,47,48]. This, combined with the analysis of the formation enthalpies ΔH and cohesive energies E_{coh} (as described above), leads us to the conclusion that alkali alanates of $MAlH_4$ (M = Li, Na, K, and Cs) containing higher χ_P are expected to use less energy for hydrogen desorption in the following hydrogen dissociation energy calculation.

3.2. Hydrogen Dissociation Energy

Dehydrogenation ability can be characterized theoretically by the hydrogen dissociation energy at which one or more hydrogen atoms are removed from a mother bulk. Table 2 lists the atomic hydrogen dissociation energies E_d-H for H_A (Equation (3)) and H_X (H_B, H_C, H_D, H_E, H_F, H_G, and H_H) removal (Equation (4)), as well as the molecular hydrogen dissociation energies E_d-H_2 for $H_A \rightarrow H_X$ (Equation (5)) and H_A–H_X removal (Equation (6)), and their minimum and average values for $MAlH_4$ (M = Li, Na, K, and Cs). As can be seen in Table 2, for atomic hydrogen H_A or H_X desorption (an asynchronous $H_A \rightarrow H_X$ process with H_A releasing first followed by the release of H_X), the energy cost for H_X desorption is much lower than that for H_A desorption, such as in $LiAlH_4$ −0.080 eV (E_d-H_B) << 1.815 eV (E_d-H_A). This indicates that it is easier for alanates of $MAlH_4$ (M = Li, Na, K, and Cs) with an H_A vacancy to release another hydrogen H_X and even induce spontaneous H_X dissociation as the hydrogen dissociation energies E_d-H_X are negative (Table 2) [49–51]. Shi et al. [52] had proposed that the hydrogen diffusion of sodium aluminum hydrides is mediated by hydrogen vacancies. Here, the favorable H_X desorption benefits from the H_A vacancy in the $MAlH_4$ bulk. For molecular hydrogen H_A and H_X desorption, on the one hand, asynchronous $H_A \rightarrow H_X$ desorption delivers a hydrogen dissociation energy very

close to that for the corresponding synchronous H_A–H_X desorption, as noted in the example of $LiAlH_4$ with E_d-H_2 = 1.735 eV ($H_A \rightarrow H_B$) and 1.733 eV (H_A–H_B). On the other hand, both asynchronous $H_A \rightarrow H_X$ and synchronous H_A–H_X desorption achieve lower hydrogen dissociation energy as H_A and H_X from two $[AlH_4]$ units compared to H_A and H_X from one $[AlH_4]$ unit, e.g., in $LiAlH_4$ E_d-H_2 = 0.953 eV ($H_A \rightarrow H_E$) vs. 1.735 eV ($H_A \rightarrow H_B$). In general, the formation of a stable $[AlH_3]$ unit/cluster followed by hydrogen release plays an important role in lowering the hydrogen removal energy in sodium alanate [53,54]. In the present work on alkali alanates of $MAlH_4$, $[AlH_3]$ units are found to form upon $H_A \rightarrow H_X$ and H_A–H_X desorption. Moreover, for a given system, the formed $[AlH_3]$ units are more stable with H_A and H_X from two $[AlH_4]$ units because, in this case, H_A and H_X desorption has lower hydrogen dissociation energy (E_d-H_2) (as described above); thus, the corresponding H_A and H_X desorbed system has lower total energy (E) according to Equations (3)–(6). This can be observed in the examples shown in Figure 3, where H_A and H_X desorption from one/two $[AlH_4]$ units has relative low hydrogen dissociation energy among all corresponding types of $H_A \rightarrow H_X$ and H_A–H_X desorption, including H_A–H_C and H_A–H_E desorption for $LiAlH_4$, H_A–H_C and $H_A \rightarrow H_F$ desorption for $NaAlH_4$, H_A–H_C and $H_A \rightarrow H_G$ desorption for $KAlH_4$, and H_A–H_D and H_A–H_G desorption for $CsAlH_4$ (Table 2). Obviously, our findings support the notion that the formation of stable $[AlH_3]$ units upon H-desorption is responsible for the reduction in the hydrogen dissociation energy in the alkali alanates of $MAlH_4$.

Table 2. The hydrogen dissociation energy of $MAlH_4$ (M = Li, Na, K, and Cs), including atomic hydrogen dissociation energy (E_d-H) for H_A and H_X (H_B, H_C, H_D, H_E, H_F, H_G, H_H) desorption and molecular hydrogen dissociation energy (E_d-H_2) for $H_A \rightarrow H_X$ (outside the bracket) and H_A–H_X desorption (inside the bracket). The minimum and average values of all E_d-H_2 are also listed.

Hydrogen Dissociation Energy (eV)		$LiAlH_4$	$NaAlH_4$	$KAlH_4$	$CsAlH_4$
Atomic hydrogen desorption E_d-H	H_A	1.815	1.719	1.702	1.720
	H_B	−0.080	−0.129	0.080	0.142
	H_C	−0.526	−0.077	−0.038	−0.006
	H_D	−0.019	−0.077	−0.037	0.000
	H_E	−0.862	−0.736	−0.721	−0.658
	H_F	−0.971	−0.747	−0.722	−0.663
	H_G	−0.788	−0.637	−0.723	−0.664
	H_H	−0.786	−0.634	−0.723	−0.665
Molecular hydrogen desorption E_d-H_2	$H_A \rightarrow H_B$ (H_A–H_B)	1.735 (1.733)	1.590 (1.592)	1.782 (1.773)	1.862 (1.866)
	$H_A \rightarrow H_C$ (H_A–H_C)	1.289 (1.287)	1.642 (1.545)	1.664 (1.661)	1.714 (1.726)
	$H_A \rightarrow H_D$ (H_A–H_D)	1.796 (1.704)	1.642 (1.660)	1.665 (1.664)	1.720 (1.708)
	$H_A \rightarrow H_E$ (H_A–H_E)	0.953 (0.832)	0.983 (0.997)	0.981 (0.984)	1.062 (1.057)
	$H_A \rightarrow H_F$ (H_A–H_F)	0.844 (0.844)	0.972 (0.975)	0.980 (0.982)	1.057 (1.055)
	$H_A \rightarrow H_G$ (H_A–H_G)	1.027 (0.856)	1.082 (1.085)	0.979 (0.986)	1.056 (1.053)
	$H_A \rightarrow H_H$ (H_A–H_H)	1.029 (1.029)	1.085 (1.081)	0.979 (0.993)	1.055 (1.065)
	Minimum value	0.832	0.972	0.979	1.053
	Average value	1.211	1.281	1.291	1.361

In Table 2, it is worth noting that the hydrogen dissociation energies E_d-H_2 of the considered hydrides of $MAlH_4$ (M = Li, Na, K, and Cs), with respect to the minimum and average values, decrease in the order of $LiAlH_4$ < $NaAlH_4$ < $KAlH_4$ < $CsAlH_4$, i.e., 0.832 eV ($LiAlH_4$) < 0.972 eV ($NaAlH_4$) < 0.979 eV ($KAlH_4$) < 1.053 eV ($CsAlH_4$), for the minimum value, and 1.211 eV ($LiAlH_4$) < 1.281 eV ($NaAlH_4$) < 1.291 eV ($KAlH_4$) < 1.361 eV ($CsAlH_4$) for the average value. These characteristics are also achieved in $M_4Al_4H_{16}$ (primitive cell) in addition to $M_8Al_8H_{32}$ (2 × 1 × 1 supercell, present work). In particular, the descending order of hydrogen dissociation energies (E_d-H_2) agrees well with that of the calculated formation enthalpies (ΔH) and cohesive energies (E_{coh}) (Table 1), as well as the experimental onset dehydriding temperature, 443 K ($LiAlH_4$) [20] < 503 K ($NaAlH_4$) [21] < 573 K ($KAlH_4$) [20] < 600 K ($CsAlH_4$) [19] (as described above). However, this order is

opposite to that of the cation electronegativity, namely, 0.98 (Li) > 0.93 (Na) > 0.82 (K) > 0.79 (Cs). The results further verify the fact that the alkali metal aluminum hydrides of $MAlH_4$ with more electronegative alkali cations are thermally less stable and, therefore, energetically favorable for hydrogen desorption.

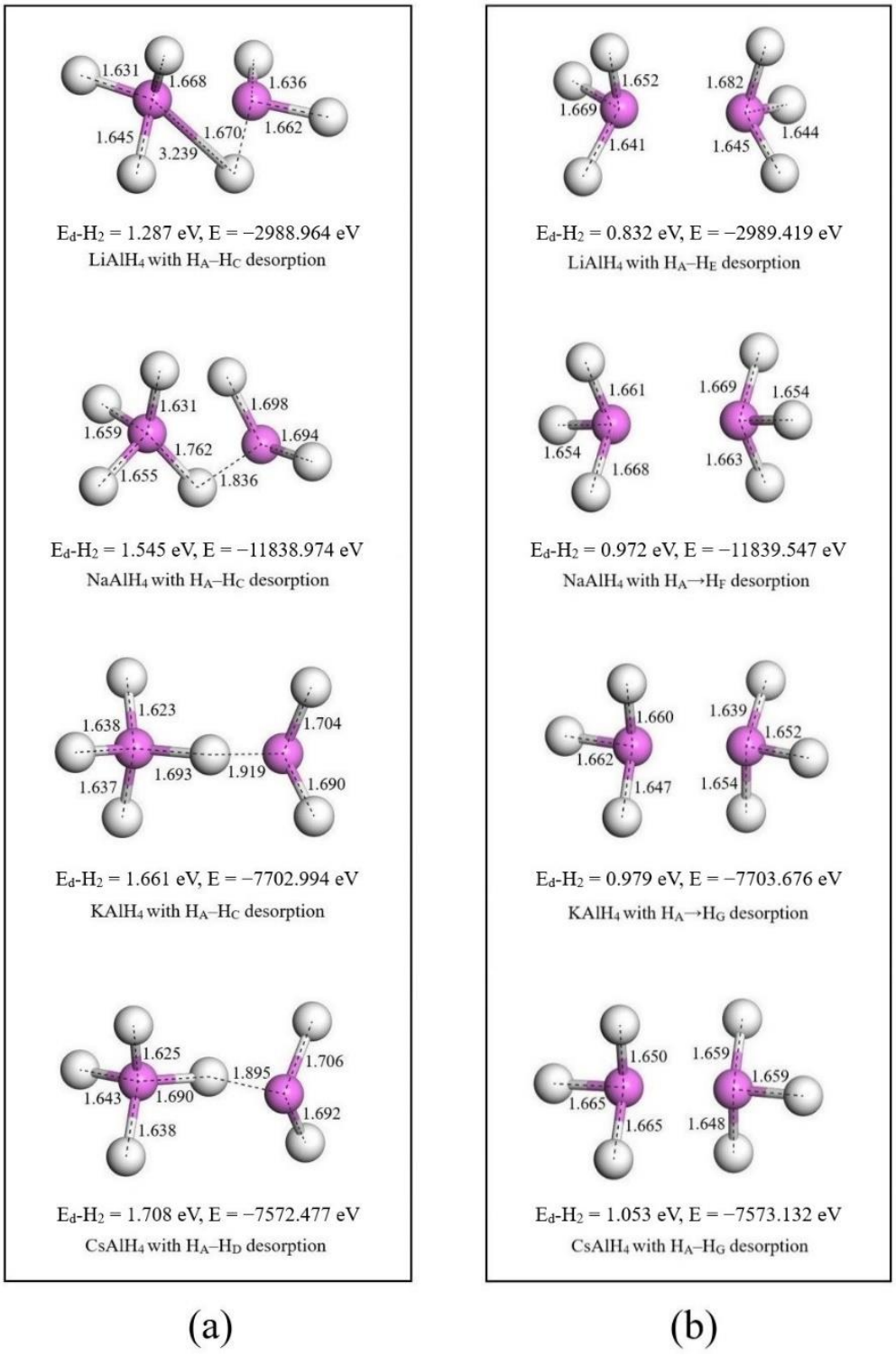

Figure 3. The formed AlH_3 group, hydrogen dissociation energy (E_d-H_2), and total energy (E) for $MAlH_4$ (M = Li, Na, K, and Cs) with H_A and H_X desorption: (**a**) H_A and H_X from one [AlH_4] unit; (**b**) H_A and H_X from two [AlH_4] units. The bond lengths between Al and H atoms in AlH_3 group are described (in Å).

3.3. Electronic Structures

As described above, Al-H and H-H bonds can be detected in the [AlH_4] groups of $MAlH_4$ (M = Li, Na, K, and Cs). Thus, upon dehydrogenation, the release of H_A or/and H_X from the considered [AlH_4] units (Figure 1) may be accompanied by the separation/rupture of Al-H and H-H bonds. In addition, weakened Al-H bonds are believed to be beneficial to the dehydrogenation of aluminum hydrides [55–57]. In consideration of these facts, determined the bonding features between Al-H and H-H according to the density of states, charge density distributions, and Mulliken populations should be help clarify the dehydriding mechanism of the alkali alanates of $MAlH_4$ (M = Li, Na, K, and Cs).

Figure 4 presents the total (TDOS) and partial density of states (PDOS) of $MAlH_4$ (M = Li, Na, K, and Cs), with a Fermi level (E_F) at 0 eV and H atoms (H_A and H_B) from the considered [AlH_4] unit in Figure 1. As can be seen, the DOS pictures of the studied hydrides of $MAlH_4$, especially M = Li, Na and K, are very similar to each other. There are orbital hybridizations between the Al and H atoms whether below Fermi level or above, thereby demonstrating a bonding interaction between Al-H. Similarly, the bonding precipitated by the interaction between H and H atoms is achieved through the hybridizations between the s states of the H atoms. These bonds of Al-H and H-H described in the DOS pictures (Figure 4) can also be detected by the charge density distribution of $MAlH_4$ (M = Li, Na, K, and Cs) (Figure 5). As shown in the Figures, the overlapping electronic clouds with appropriate distances between Al and H atoms (1.625–1.641 Å), and H and H atoms (2.650–2.721 Å) in Figure 5, may contribute to the formation of Al-H and H-H bonds, respectively [31,40]. In the DOS pictures, it is worth noting that the peaks of the TDOS contribution from Al and H electronic states (marked as I and II in Figure 4) tend to increase at lower cation electronegativity due to the enhanced PDOS of Al s and *p* states and H s states (such as $KAlH_4$ and $CsAlH_4$), so one or both Al-H and H-H bonding interactions may become stronger with a decreasing cation electronegativity [50,51,58].

To further quantitatively elucidate the bonding characteristics between Al-H and H-H, a Mulliken population analysis was performed on the $MAlH_4$ (M = Li, Na, K, and Cs) compounds. The results, including the average bond order (BO), the average bond length (BL), and the scaled bond order (BO^s) between Al-H and H-H, are listed in Table 3. Here, BO indicates the overlapping electron population between atoms, and is useful when considering bonding characteristics with an ionic (BO < 0, BO = 0) or covalent nature (BO > 0) [40,41,58–61]. BO^s, defined as $BO^s = BO/BL$, is helpful for assessing the relative bonding strength between atoms. A bond with a higher BO^s value is expected to be stronger [40,41,58]. It can be seen from Table 3 that for all the studied compounds, Al-H bonds with a positive bond order ($BO_{Al\text{-}H} > 0$) show a covalent character, while H-H bonds with a negative bond order ($BO_{H\text{-}H} < 0$) exhibit an ionic nature. The H-H ionic interactions were found to be weakened at a higher electronegativity of the cation M. As shown, the scaled bond order between H-H ($BO^s_{H\text{-}H}$) decreases linearly (-0.013 $Å^{-1}$ ($LiAlH_4$) < -0.014 $Å^{-1}$ ($NaAlH_4$) < -0.021 $Å^{-1}$ ($KAlH_4$) < -0.022 $Å^{-1}$ ($CsAlH_4$)) with the increase in cation electronegativity (0.98 (Li) > 0.93 (Na) > 0.82 (K) > 0.79 (Cs)). The trend of the Al-H covalent interactions among the studied aluminum hydrides (except $CsAlH_4$) is similar to that of the H-H ionic interactions. Araújo et al. [55] reported that hydrogen atoms held by weak covalent and ionic bonds may lead to lower dissociation temperatures for complex alkali metal aluminum hydrides. In addition, many previous studies have shown that reducing the Al-H covalent bonding strength in metal aluminum hydrides facilitates their decomposition for H-desorption [55–57,62]. Our calculated results with respect to $MAlH_4$ (M = Li, Na, K, and Cs) mainly support these findings. That is, aluminum hydrides of $MAlH_4$ with larger cation electronegativity and weaker H-H ionic and Al-H covalent interactions exhibit lower hydrogen dissociation energies (Table 2). As an example, the $LiAlH_4$ hydride containing the weakest H-H ionic ($BO^s_{H\text{-}H} = -0.013$ $Å^{-1}$, Table 3) and the Al-H covalent interactions ($BO^s_{Al\text{-}H} = 0.476$ $Å^{-1}$, Table 3) show the lowest hydrogen dissociation energies for hydrogen desorption (E_d-H_2 = 1.211 eV, Table 2) relative to the other three hydrides, namely, $NaAlH_4$, $KAlH_4$, and $CsAlH_4$. The results described above

lead us to the conclusion that weakening the ionic and covalent H bonds (such as H-H ionic and Al-H covalent bonds) by increasing cation electronegativity helps to modify the dehydrogenation performance of the alkali metal aluminum hydrides of $MAlH_4$ (M = Li, Na, K, and Cs). The incorporation of more electronegative elements (compared to M) into the $MAlH_4$ bulk could be used for this purpose.

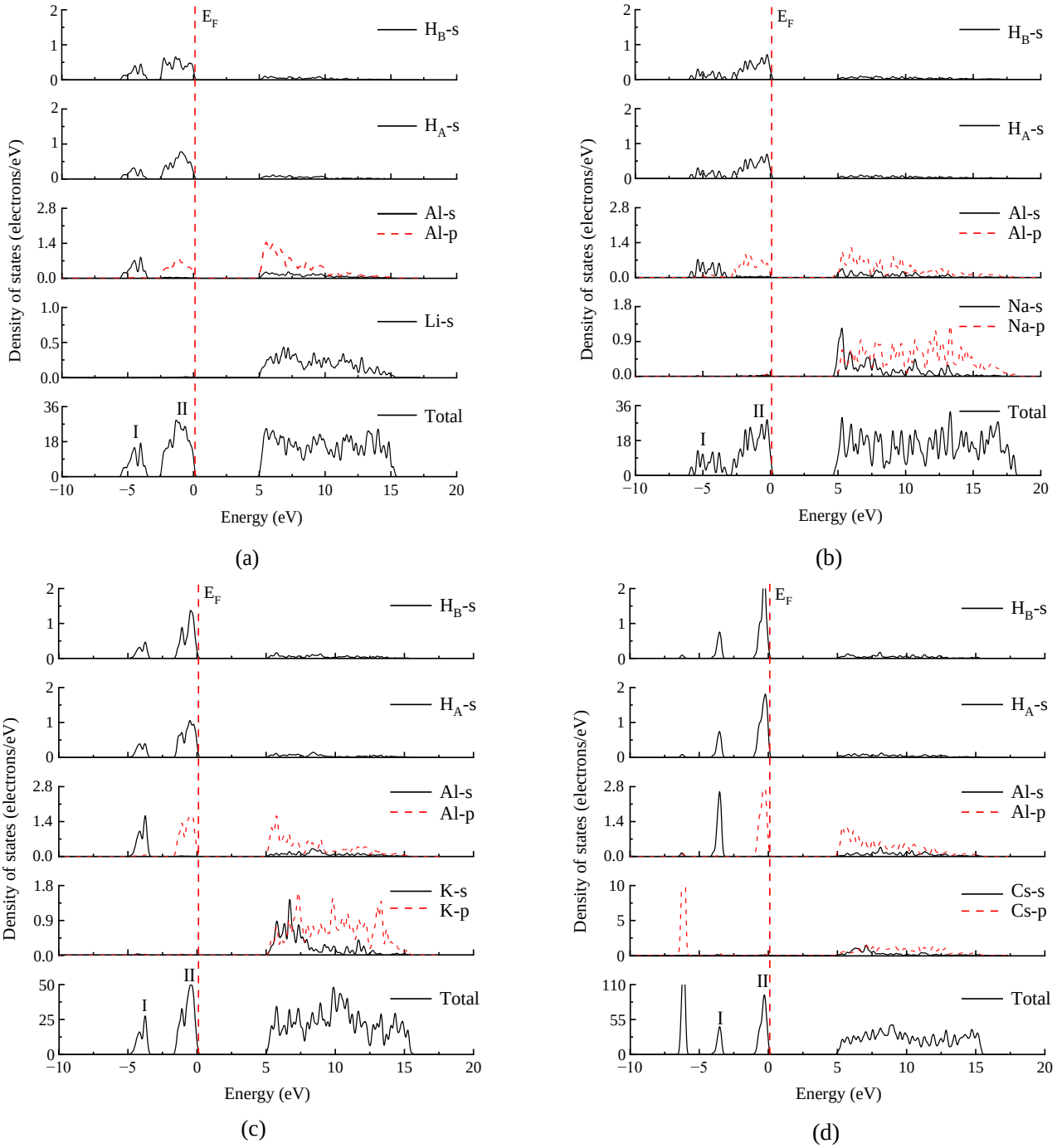

Figure 4. The total (TDOS) and partial density of states (PDOS) for $MAlH_4$ (M = Li, Na, K, and Cs), with Fermi level (E_F, marked with vertical dotted line) at 0 eV and H atoms (H_A and H_B) from considered [AlH_4] unit in Figure 1: (**a**) $LiAlH_4$, (**b**) $NaAlH_4$, (**c**) $KAlH_4$, and (**d**) $CsAlH_4$. The TDOS labeled by I and II are mainly contributed by Al and H electronic states.

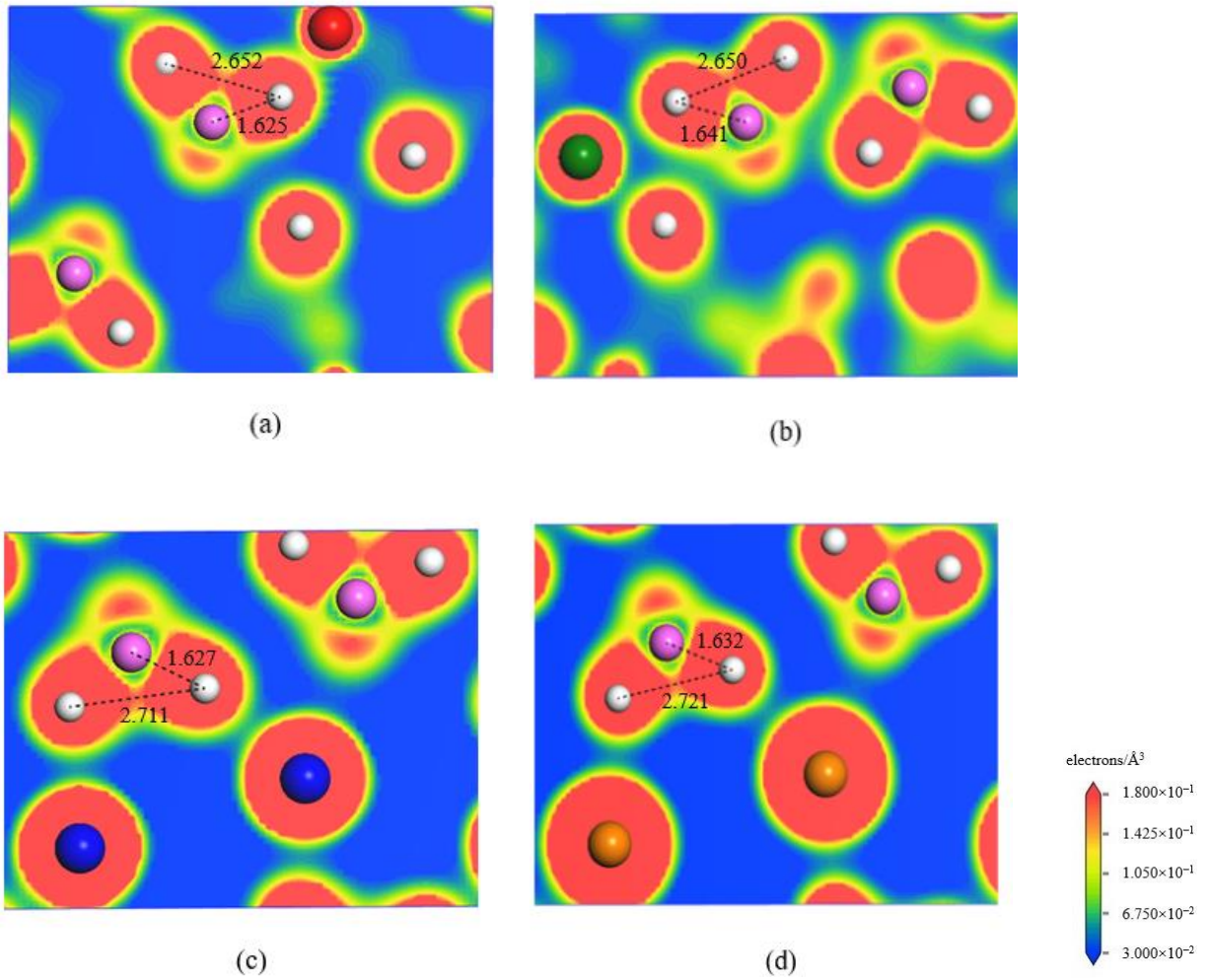

Figure 5. The electronic density contours for $MAlH_4$ (M = Li, Na, K, and Cs) with the contour line from 0.03 to 0.18 electrons/Å^3: (**a**) $LiAlH_4$, (**b**) $NaAlH_4$, (**c**) $KAlH_4$, and (**d**) $CsAlH_4$. Li, Na, K, Cs, Al, and H atoms are denoted by red, green, blue, orange, pink, and white spheres, respectively. The shortest distances between Al and H atoms and H and H atoms in this figure are described (in Å).

Table 3. The Mulliken population for $MAlH_4$ (M = Li, Na, K, and Cs), including the average bond order (BO), average bond length (BL), and scaled bond order (BO^s) between Al-H and H-H.

Compounds	Al-H			H-H		
	BO	BL (Å)	BO^S (Å^{-1})	BO	BL (Å)	BO^S (Å^{-1})
$LiAlH_4$	0.778	1.634	0.476	−0.036	2.751	−0.013
$NaAlH_4$	0.855	1.642	0.521	−0.039	2.755	−0.014
$KAlH_4$	0.906	1.634	0.555	−0.055	2.668	−0.021
$CsAlH_4$	0.893	1.637	0.545	−0.058	2.673	−0.022

4. Conclusions

First-principles calculations were performed on the alkali alanates of $MAlH_4$ (M = Li, Na, K, and Cs) to investigate their thermal stability, hydrogen dissociation energy, and electronic structures. The results show that cation electronegativity (χ_P) is a good indicator with which to assess the thermal stability and dehydrogenation ability of $MAlH_4$ (M = Li, Na, K, and Cs). For $MAlH_4$ with a higher χ_P, on the one hand, it is thermally less stable because the formation enthalpy ΔH and cohesive energy E_{och} become less negative and the $M^+ \rightarrow [AlH_4]^-$ charge transfer is suppressed. On the other hand, it is energetically favorable for hydrogen desorption ($H_A \rightarrow H_X$ and H_A–H_X, especially H_A and H_X from two $[AlH_4]$

units), which is associated with its poor stability and weaker H-H ionic and Al-H covalent interactions. Our work provides new insights into the dehydrogenation of $MAlH_4$ (M = Li, Na, K, and Cs) and is useful for designing advanced aluminum hydrides with favorable H-desorption properties.

Author Contributions: Conceptualization, R.Z. and W.J.; Methodology, R.Z., X.M., Y.H., C.H. and W.J.; Data Curation, R.Z., X.M., Y.H., C.H. and X.Z.; Formal Analysis, R.Z., X.M. and W.J.; Validation, R.Z., Y.H., X.Z., Y.M. and Q.W.; Funding Acquisition, W.J.; Writing—Original Draft, R.Z. and W.J.; Supervision, X.M. and W.J.; Writing—Review and Editing, W.J. All authors have read and agreed to the published version of the manuscript.

Funding: This work was funded by the National Natural Science Foundation of China (51661002), and the Natural Science Foundation of Guangxi (2018GXNSFAA138189).

Data Availability Statement: The data presented in this study are available on request from the corresponding author.

Acknowledgments: This work was supported by the National Natural Science Foundation of China (51661002), the Natural Science Foundation of Guangxi (2018GXNSFAA138189), and the high-performance computing platform of Guangxi University.

Conflicts of Interest: The authors declare no conflict of interest.

References

1. Schlapbach, L.; Züttel, A. Hydrogen-storage materials for mobile applications. *Nature* **2001**, *414*, 353–358. [CrossRef] [PubMed]
2. Zhu, M.; Lu, Y.S.; Ouyang, L.Z.; Wang, H. Thermodynamic tuning of Mg-based hydrogen storage alloys: A review. *Materials* **2013**, *6*, 4654–4674. [CrossRef] [PubMed]
3. Rusman, N.A.A.; Dahari, M. A review on the current progress of metal hydrides material for solid-state hydrogen storage applications. *Int. J. Hydrogen Energy* **2016**, *41*, 12108–12126. [CrossRef]
4. Li, L.; Huang, Y.K.; An, C.H.; Wang, Y.J. Lightweight hydrides nanocomposites for hydrogen storage: Challenges, progress and prospects. *Sci. China Mater.* **2019**, *62*, 1597–1625. [CrossRef]
5. Ali, N.A.; Ismail, M. Modification of $NaAlH_4$ properties using catalysts for solid-state hydrogen storage: A review. *Int. J. Hydrogen Energy* **2021**, *46*, 766–782. [CrossRef]
6. Li, H.W.; Orimo, S.; Nakamori, Y.; Miwa, K.; Ohba, N.; Towata, S.; Züttel, A. Materials designing of metal borohydrides: Viewpoints from thermodynamical stabilities. *J. Alloys Compd.* **2007**, *446–447*, 315–318. [CrossRef]
7. Ren, Z.H.; Zhang, X.; Huang, Z.G.; Hu, J.J.; Li, Y.Z.; Zheng, S.Y.; Gao, M.X.; Pan, H.G.; Liu, Y.F. Controllable synthesis of 2D TiH_2 nanoflakes with superior catalytic activity for low-temperature hydrogen cycling of $NaAlH_4$. *Chem. Eng. J.* **2022**, *427*, 131546. [CrossRef]
8. Guo, Y.H.; Yu, X.B.; Gao, L.; Xia, G.L.; Guo, Z.P.; Liu, H.K. Significantly improved dehydrogenation of $LiBH_4$ destabilized by TiF_3. *Energy Environ. Sci.* **2010**, *3*, 465–470. [CrossRef]
9. Li, Y.; Zhang, Y.; Gao, M.X.; Pan, H.G.; Liu, Y.F. Preparation and catalytic effect of porous Co_3O_4 on the hydrogen storage properties of a Li-B-N-H system. *Prog. Nat. Sci.-Mater.* **2017**, *27*, 132–138. [CrossRef]
10. Wei, S.; Liu, J.X.; Xia, Y.P.; Zhang, H.Z.; Cheng, R.G.; Sun, L.X.; Xu, F.; Huang, P.R.; Rosei, F.; Pimerzin, A.A.; et al. Remarkable catalysis of spinel ferrite XFe_2O_4 (X = Ni, Co, Mn, Cu, Zn) nanoparticles on the dehydrogenation properties of $LiAlH_4$: An experimental and theoretical study. *J. Mater. Sci. Technol.* **2022**, *111*, 189–203. [CrossRef]
11. Nakamori, Y.; Miwa, K.; Ninomiya, A.; Li, H.W.; Ohba, N.; Towata, S.; Züttel, A.; Orimo, S. Correlation between thermodynamical stabilities of metal borohydrides and cation electronegativites: First-principles calculations and experiments. *Phys. Rev. B* **2006**, *74*, 045126. [CrossRef]
12. Nakamori, Y.; Li, H.W.; Kikuchi, K.; Aoki, M.; Miwa, K.; Towata, S.; Orimo, S. Thermodynamical stabilities of metal-borohydrides. *J. Alloys Compd.* **2007**, *446–447*, 296–300. [CrossRef]
13. Zhang, B.J.; Liu, B.H. Hydrogen desorption from $LiBH_4$ destabilized by chlorides of transition metal Fe, Co, and Ni. *Int. J. Hydrogen Energy* **2010**, *35*, 7288–7294. [CrossRef]
14. Mo, X.H.; Jiang, W.Q. Dehydrogenation properties of $LiBH_4$ modified by Mg from first-principles calculations. *J. Alloys Compd.* **2018**, *735*, 668–676. [CrossRef]
15. Cai, W.T.; Yang, Y.Z.; Tao, P.J.; Ouyang, L.Z.; Wang, H. Correlation between structural stability of $LiBH_4$ and cation electronegativity in metal borides: An experimental insight for catalyst design. *Dalton Trans.* **2018**, *47*, 4987–4993. [CrossRef] [PubMed]
16. Chen, X.; Li, Z.; Zhang, Y.; Liu, D.M.; Wang, C.Y.; Li, Y.T.; Si, T.Z.; Zhang, Q.G. Enhanced low-temperature hydrogen storage in nanoporous Ni-based alloy supported $LiBH_4$. *Front. Chem.* **2020**, *8*, 283. [CrossRef] [PubMed]
17. Nakamori, Y.; Orimo, S.I. Destabilization of Li-based complex hydrides. *J. Alloys Compd.* **2004**, *370*, 271–275. [CrossRef]

18. Bai, Y.; Pei, Z.W.; Wu, F.; Wu, C. Role of metal electronegativity in the dehydrogenation thermodynamics and kinetics of composite metal borohydride-$LiNH_2$ hydrogen storage materials. *ACS Appl. Mater. Interfaces* **2018**, *10*, 9514–9521. [CrossRef] [PubMed]
19. Weidenthaler, C. Crystal structure evolution of complex metal aluminum hydrides upon hydrogen release. *J. Energy Chem.* **2020**, *42*, 133–143. [CrossRef]
20. Mamatha, M.; Weidenthaler, C.; Pommerin, A.; Felderhoff, M.; Schüth, F. Comparative studies of the decomposition of alanates followed by in situ XRD and DSC methods. *J. Alloys Compd.* **2006**, *416*, 303–314. [CrossRef]
21. Finholt, A.E.; Barbaras, G.D.; Barbaras, G.K.; Urry, G.; Wartik, T.; Schlesinger, H.I. The preparation of sodium and calcium aluminum hydrides. *J. Inorg. Nucl. Chem.* **1955**, *1*, 317–325. [CrossRef]
22. Nyahuma, F.M.; Zhang, L.T.; Song, M.C.; Lu, X.; Xiao, B.B.; Zheng, J.G.; Wu, F.Y. Significantly improved hydrogen storage behaviors in MgH_2 with Nb nanocatalyst. *Int. J. Min. Met. Mater.* **2022**, *29*, 1788–1797. [CrossRef]
23. Liu, Y.; Huang, Z.N.; Gao, X.; Wang, Y.Q.; Wang, F.; Zheng, S.S.; Guan, S.N.; Yan, H.L.; Yang, X.; Jia, W.H. Effect of novel La-based alloy modification on hydrogen storage performance of magnesium hydride: First-principles calculation and experimental investigation. *J. Power Sources* **2022**, *551*, 232187. [CrossRef]
24. Segall, M.D.; Lindan, P.J.D.; Probert, M.J.; Pickard, C.J.; Hasnip, P.J.; Clark, S.J.; Payne, M.C. First-principles simulation: Ideas, illustrations and the CASTEP code. *J. Phys. Condes. Matter* **2002**, *14*, 2717–2744. [CrossRef]
25. Perdew, J.P.; Burke, K.; Ernzerhof, M. Generalized gradient approximation made simple. *Phys. Rev. Lett.* **1996**, *77*, 3865–3868. [CrossRef] [PubMed]
26. Pfrommer, B.G.; Côté, M.; Louie, S.G.; Cohen, M.L. Relaxation of crystals with the quasi-newton method. *J. Comput. Phys.* **1997**, *131*, 233–240. [CrossRef]
27. Hauback, B.C.; Brinks, H.W.; Fjellvåg, H. Accurate structure of $LiAlD_4$ studied by combined powder neutron and X-ray diffraction. *J. Alloys Compd.* **2002**, *346*, 184–189. [CrossRef]
28. Ozolins, V.; Majzoub, E.H.; Udovic, T.J. Electronic structure and Rietveld refinement parameters of Ti-doped sodium alanates. *J. Alloys Compd.* **2004**, *375*, 1–10. [CrossRef]
29. Hauback, B.C.; Brinks, H.W.; Heyn, R.H.; Blom, R.; Fjellvåg, H. The crystal structure of $KAlD_4$. *J. Alloys Compd.* **2005**, *394*, 35–38. [CrossRef]
30. Bernert, T.; Krech, D.; Kockelmann, W.; Felderhoff, M.; Frankcombe, T.J.; Weidenthaler, C. Crystal structure relation between tetragonal and orthorhombic $CsAlD_4$: DFT and time-of-flight neutron powder diffraction studies. *Eur. J. Inorg. Chem.* **2015**, *2015*, 5545–5550. [CrossRef]
31. Sirsch, P.; Che, F.N.; Titah, J.T.; McGrady, G.S. Hydride-hydride bonding interactions in the hydrogen stoage materials AlH_3, MgH_2, and $NaAlH_4$. *Chem. Eur. J.* **2012**, *18*, 9476–9480. [CrossRef]
32. Sorte, E.G.; Emery, S.B.; Majzoub, E.H.; Ellis-Caleo, T.; Ma, Z.L.; Hammann, B.A.; Hayes, S.E.; Bowman, R.C.; Conradi, M.S. NMR Study of Anion Dynamics in Solid $KAlH_4$. *J. Phys. Chem. C* **2014**, *118*, 5725–5732. [CrossRef]
33. Ravindran, P.; Vajeeston, P.; Vidya, R.; Fjellvåg, H.; Kjekshus, A. Modeling of hydrogen storage materials by density-functional calculations. *J. Power Sources* **2006**, *159*, 88–99. [CrossRef]
34. Setten, M.J.V. Electronic structure and formation enthalpy of hydroaluminates and hydroborates. *Encycl. Mater. Sci. Technol.* **2008**, *043152*, 1–6.
35. Fukai, Y. *The Metal-Hydrogen System*; Volume 21 of Springer Series in Material Science; Springer: Berlin/Heidelberg, Germany, 1993.
36. Shi, B.; Song, Y. Influence of transition metals Fe, Ni, and Nb on dehydrogenation characteristics of $Mg(BH_4)_2$: Electronic structure mechanisms. *Int. J. Hydrogen Energy* **2013**, *38*, 6417–6424. [CrossRef]
37. Zhang, J.; Sun, L.Q.; Zhou, Y.C.; Peng, P. Dehydrogenation thermodynamics of magnesium hydride doped with transition metals: Experimental and theoretical studies. *Comput. Mater. Sci.* **2015**, *98*, 211–219. [CrossRef]
38. Kumar, A.; Muthukumar, P.; Sharma, P.; Kumar, E.A. Absorption based solid state hydrogen storage system: A review. *Sustain. Energy Technol. Assess.* **2022**, *52*, 102204. [CrossRef]
39. Zhao, L.; Xu, F.; Zhang, C.C.; Wang, Z.Y.; Ju, H.Y.; Gao, X.; Zhang, X.X.; Sun, L.X.; Liu, Z.W. Enhanced hydrogen storage of alanates: Recent progress and future perspectives. *Prog. Nat. Sci.* **2021**, *31*, 165–179. [CrossRef]
40. Mo, X.H.; Liang, J.Q.; Wang, W.H.; Jiang, W.Q. First-principles study on the dehydrogenation of $Li_4BN_3H_{10}$ modified by Co. *Int. J. Hydrogen Energy* **2021**, *46*, 11815–11823. [CrossRef]
41. Jiang, W.Q.; Chen, Y.J.; Mo, X.H.; Li, X.L. First-principles investigation of $LaMg_2Ni$ and its hydrides. *Sci. Rep.* **2020**, *10*, 12167. [CrossRef]
42. Jiang, W.Q.; Qin, C.S.; Zhu, R.R.; Guo, J. Annealing effect on hydrogen storage property of Co-free $La_{1.8}Ti_{0.2}MgNi_{8.7}Al_{0.3}$ alloy. *J. Alloys Compd.* **2013**, *565*, 37–43. [CrossRef]
43. Wang, H.Y.; Zhang, N.; Wang, C.; Jiang, Q.C. First-principles study of the generalized stacking fault energy in Mg-3Al-3Sn alloy. *Scr. Mater.* **2011**, *65*, 723–726. [CrossRef]
44. Løvvik, O.M.; Opalka, S.M.; Brinks, H.W.; Hauback, B.C. Crystal structure and thermodynamic stability of the lithium alanates $LiAlH_4$ and Li_3AlH_6. *Phys. Rev. B* **2004**, *69*, 134117. [CrossRef]
45. Lide, D.R. *CRC Handbook of Chemistry and Physics*, 80th ed.; CRC Press: Boca Raton, FL, USA, 2000.
46. Wang, X.; Yu, X.H.; Zhong, Y.; Rong, J.; Li, X.Y.; Feng, J.; Zhan, Z.L. Stability and mechanical peroperties of high-La content La-Ni phases by first-principles study. *Int. J. Mod. Phys. B* **2018**, *32*, 1850242. [CrossRef]

47. Miwa, K.; Ohba, N.; Towata, S.; Nakamori, Y.; Orimo, S. First-principles study on lithium borohydride $LiBH_4$. *Phys. Rev. B* **2004**, *69*, 245120. [CrossRef]
48. Miwa, K.; Ohba, N.; Towata, S.; Nakamori, Y.; Orimo, S. First-principles study on copper-substituted lithium borohydride, $(Li_{1-x}Cu_x)BH_4$. *J. Alloys Compd.* **2005**, *404–406*, 140–143. [CrossRef]
49. Dai, J.H.; Song, Y.; Yang, R. Intrinsic mechanisms on enhancement of hydrogen desorption from MgH_2 by (001) surface doping. *Int. J. Hydrogen Energy* **2011**, *36*, 12939–12949. [CrossRef]
50. Mo, X.H.; Long, L.X.; Tan, W.B.; Huang, Y.P.; Lu, J.W.; Zhao, Y.W.; Jiang, W.Q. First-principles investigation of dehydrogenation of Cu-doped $LiBH_4$. *Solid State Commun.* **2021**, *326*, 114184. [CrossRef]
51. Mo, X.H.; Jiang, W.Q.; Cao, S.L. First-principles study on the dehydrogenation characteristics of $LiBH_4$ modified by Ti. *Results Phys.* **2017**, *7*, 3236–3242. [CrossRef]
52. Shi, Q.; Voss, J.; Jacobsen, H.S.; Lefmann, K.; Zamponi, M.; Vegge, T. Point defect dynamics in sodium aluminum hydrides–a combined quasielastic neutron scattering and density functional theory study. *J. Alloys Compd.* **2007**, *446–447*, 469–473. [CrossRef]
53. Araújo, C.M.; Li, S.; Ahuja, R.; Jena, P. Vacancy-mediated hydrogen desorption in $NaAlH_4$. *Phys. Rev. B* **2005**, *72*, 165101. [CrossRef]
54. Wang, H.; Tezuka, A.; Ogawa, H.; Ikeshoji, T. First-principles study of hydrogen vacancies in sodium alanate with Ti substitution. *J. Phys. Condes. Matter* **2010**, *22*, 205503. [CrossRef]
55. Araújo, C.M.; Ahuja, R.; Guillén, J.M.O.; Jena, P. Role of titanium in hydrogen desorption in crystalline sodium alanate. *Appl. Phys. Lett.* **2005**, *86*, 251913. [CrossRef]
56. Zhang, X.; Ren, Z.H.; Zhang, X.L.; Gao, M.X.; Pan, H.G.; Liu, Y.F. Triggering highly stable catalytic activity of metallic titanium for hydrogen storage in $NaAlH_4$ by preparing ultrafine nanoparticles. *J. Mater. Chem. A* **2019**, *7*, 4651–4659. [CrossRef]
57. Liu, Z.Y.; Liu, J.X.; Wei, S.; Xia, Y.P.; Cheng, R.G.; Sun, L.X.; Xu, F.; Huang, P.R.; Bu, Y.T.; Cheng, J.; et al. Improved hydrogen storage properties and mechanisms of $LiAlH_4$ doped with Ni/C nanoparticles anchored on large-size $Ti_3C_2T_x$. *J. Alloys Compd.* **2023**, *931*, 167353. [CrossRef]
58. Jiang, W.Q.; Cao, S.L. Effect of Al on the dehydrogenation of $LiBH_4$ from first-principles calculations. *Int. J. Hydrogen Energy* **2017**, *42*, 6181–6188.
59. Segall, M.D.; Shah, R.; Pickard, C.J.; Payne, M.C. Population analysis of plane-wave electronic structure calculations of bulk materials. *Phys. Rev. B* **1996**, *54*, 16317–16320. [CrossRef]
60. Wang, H.P.; Wang, X.M.; Ge, F.F.; Zhou, M.J.; Wu, W.D.; Lu, T.C. Density function study of H_2 adsorption on LiB (010) surface. *Phys. B* **2010**, *405*, 1792–1795.
61. Zhu, C.Y.; Liu, Y.H.; Duan, D.F.; Cui, T. Structural transitions of $NaAlH_4$ under high pressure by first-principles calculations. *Phys. B* **2011**, *406*, 1612–1614. [CrossRef]
62. Berseth, P.A.; Harter, A.G.; Zidan, R.; Blomqvist, A.; Araújo, C.M.; Scheicher, R.H.; Ahuja, R.; Jena, P. Carbon nanomaterials as catalysts for hydrogen uptake and release in $NaAlH_4$. *Nano Lett.* **2009**, *9*, 1501–1505. [CrossRef]

Disclaimer/Publisher's Note: The statements, opinions and data contained in all publications are solely those of the individual author(s) and contributor(s) and not of MDPI and/or the editor(s). MDPI and/or the editor(s) disclaim responsibility for any injury to people or property resulting from any ideas, methods, instructions or products referred to in the content.